



# Experimental and computational study on the mechanism of iodine vapour adsorption by modified activated carbon fibers at different scales

Xiaomin Yang<sup>1,2</sup> · Hui Wu<sup>2,3</sup> · Dong Xie<sup>2,3</sup>

Received: 24 February 2023 / Accepted: 29 August 2023 / Published online: 17 October 2023  
© Akadémiai Kiadó, Budapest, Hungary 2023

## Abstract

The effective capture of iodine vapour, a potential threat of environment and human health, is crucial for efficiently managing nuclear waste gases. Herein, the adsorption property of iodine vapour on modified activated carbon fibers was investigated using adsorption experiment and simulation methods, to explain the adsorption mechanism at different scales. Preliminary results hint that the ideal adsorbent should have lower density, higher adsorption coefficient and taller porosity, and more pores between 1.6 and 1.9 nm. Compared with KOH modification, microwave modification can effectively improve the performance of activated carbon fibers for capturing iodine vapour.

**Keywords** Iodine vapour · Modified activated carbon fibers · COMSOL simulation · GCMC simulation

## Introduction

Nuclear energy is a main alternative source to meet the energy demands due to its safe, clean, reliable and cheap [1]. Despite this, the growth of the nuclear energy may be limited by the radioactive waste produced management, due to a huge amount of radioactive waste gases are produced amid handling the spent fuel, such as iodine (<sup>129</sup>I), krypton (<sup>85</sup>Kr), and tritium (<sup>3</sup>H) [2–4], which should be captured immediately to protect human health and environment. Among these waste gases, radioactive iodine is the largest part of the releases [5], for example  $3.2 \times 10^5$  g of <sup>129</sup>I each year will be liberated from a nuclear fuel reprocessing plant with 5 tons/day of production capacity. Consequently, it is necessary to effectively capture iodine from the nuclear off-gas streams to control their emission.

Adsorption is one of the effective avenue to capture iodine vapour, attributing to that it is a mature, simple, reliable, non-corrosive, low maintenance and operation cost technology. Although AgS [6], silver nitrate-silica gel [7, 8], and nano-sodium titanate ETS-2 deposited silver [9] were prepared to efficiently capture iodine under different conditions, they are hampered by costly price and toxic nature of silver. Other adsorbents, like metal-organic frameworks (MOFs) [10], nanostructured C@ETS-10 sorbent [3], Chalcogenide aerogels [11] and porous organic frameworks (POFs) [12, 13], have also been investigated for iodine capture. Nevertheless, the low yield, high cost, and complex preparation process renders the sorbents less attractive to potential commercial application.

Activated carbon fibers (ACFs) have shown potential for iodine vapour adsorption attribute to tunable pore size distribution, high specific surface area, abundant micropores, excellent adsorption performance and good physical-chemical stability in radiation environment. Jiao et al. [14] used four types of steams and Na<sub>2</sub>CO<sub>3</sub>-K<sub>2</sub>CO<sub>3</sub> mixture as activating agents to prepare ACFs for iodine solution adsorption. H. Zhu et al. [15] synthesized Catechin@ACF with a catechin membrane on the ACFs for iodine entrapment under the relatively complicated synthesis steps. A host of simple modification methods on commercial ACFs have been carried out by thermal oxidation [16], microwave treatment [17, 18], biological modification [19], non-thermal plasma [20],

✉ Dong Xie  
nhxiedong@126.com

<sup>1</sup> School of Resource Environment and Safety Engineering, University of South China, Hengyang 421001, China

<sup>2</sup> National and Local Joint Engineering Research Center of Airborne Pollutants Treatment and Radioactive Protection in Building Environment, Hengyang 421001, China

<sup>3</sup> School of Civil Engineering, University of South China, Hengyang 421001, China

ammonia treatment [21], ozone treatment and alkaline treatment [22], which mainly were applied on water treatment.

When searching for the best preparation parameters of ACFs to capture iodine, the traditional method is a great quantity experiments to try and mainly explained the adsorption mechanism via various instrument characterization, which is uncertain, time consuming and high cost. Recently, there are an array of studies on the prediction of H<sub>2</sub>S [23], CO<sub>2</sub> [24, 25], and VOCs [26] adsorption using independently COMSOL software and GCMC molecular simulation. If the mechanism between the physicochemical characteristic of ACFs and iodine, namely structure–property relationship, is elucidated at micro and molecular levels, so the direction of preparation or modification of activated carbon fiber will be clearer. Nevertheless, the mechanism of iodine adsorption on modified ACFs using COMSOL and GCMC simulation together lacked consideration [27, 28].

In order to explore the mechanism of how density, adsorption coefficient, poriness and pore structure of ACFs impact on adsorption iodine at micro and molecular levels, a conjunct experimental and computational method was required. This included SEM, BET, element analyzer, FT-IR, COMSOL simulation and GCMC simulation. Firstly, three modified ACFs were prepared and the adsorption of iodine vapour on them was carried out by static adsorption experiment. Secondly, a model of static adsorption experiment was built using COMSOL to reveal the relationship between ACFs parameter and adsorption function at a micro level. Thirdly, a slit-like pore model of ACFs was developed and GCMC was used to figure iodine adsorption isotherm to explore the structure – function relationship at a molecular level. The overarching aim of this work was to give some feasible recommendations on select the suitable ACFs for capturing iodine vapour.

## Experimental section

### Preparation of modified ACFs

As shown in Fig. 1, the original viscose-based activated carbon fibers were cut into 2 cm × 2 cm fragments, boiled in deionized water for 1.5 h, washed with deionized water at room temperature, dried at 110 °C for 10 h and dubbed ACF-0. 20 g ACF-0 was added into 200 mL KOH solution (0.1%), and the mixtures were placed in a constant temperature water bath at 40 °C for 24 h. Then the products were washed with deionized water, dried at 110 °C for 24 h in air dry oven and denoted by ACF-K. 10 g ACF-0 was taken under microwave power at 385 W for 1 min and marked as ACF-W. 10 g ACF-K was carried out under microwave power at 385 W for 1 min and named ACF-KW.

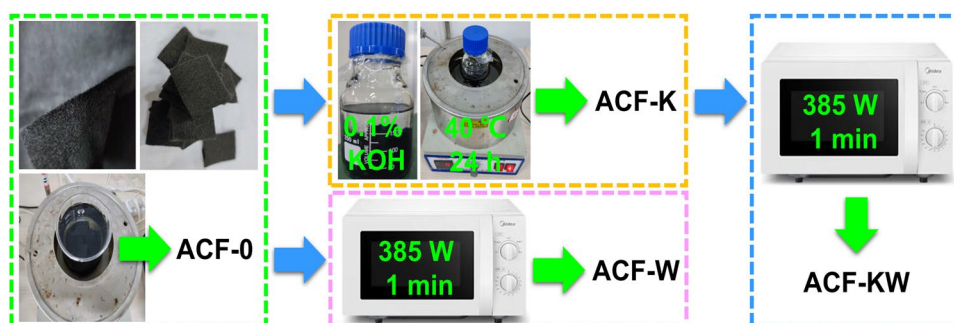
### Characterization

The microstructure of ACFs were obtained using scanning electron microscope (SEM, viewing model F50, FEI Co., Ltd., USA). N<sub>2</sub> adsorption/desorption isotherms were performed at 77 K using specific surface area porosity analyzer (BET, ASAP 2020, American Mike Instrument Co., Ltd.). The chemical elements of ACFs were analyzed using element analyzer (UNICUBE, Alymonta Co., Ltd.). The functional groups of ACFs were measured by Fourier transform infrared spectrometer (FT-IR, Nicolet-iS10, Thermo Fisher, USA).

### Static adsorption and desorption experiment of iodine vapour

ACFs samples were exposed to saturated iodine vapour. Stable iodine was used in this experiment because its physiochemical performances are similar with radioactive iodine [29–31]. 1 g ACFs and 7 g iodine were placed in a 500 mL glass vessel at 40 °C and 1 bar in water bath. The weight of iodine-loaded ACFs were measured after a certain exposure times (4–60 h). The iodine adsorption

**Fig. 1** Preparation process of pristine ACF-0 and modified ACFs (ACF-W, ACF-K, and ACF-KW)



amount was calculated gravimetrically using formula  $q = 1000 \times (m_t - m_0)/m_0$ .  $m_0$  is the initial mass of ACFs.  $m_t$  is the mass of ACFs after iodine capture at different time.

To evaluate the iodine retention performance, ACFs@I<sub>2</sub> were placed in the laboratory fume hoods at room temperature (25.3–28.4 °C) for desorption experiment.

### Adsorption kinetics models

To analyze the mechanism of adsorption, five kinetics models were investigated, namely pseudo-first-order model, pseudo-second-order model, Elovich model, Bangham model, and Intraparticle diffusion model, as shown in Table 1. Pseudo first-order adsorption kinetics model uses Lagergren equation to calculate adsorption rate and is determined physical adsorption of surface. Pseudo-second-order model is based on the adsorption rate control step of chemical reactions or chemical adsorption through electron sharing or electron gain and loss. Elovich model describes a series of reaction mechanisms, such as the diffusion of adsorbate molecules at the adsorption interface, activation of the adsorbent surface, and deactivation. Bangham model is applicable to the dynamic adsorption process of gas molecules on solid adsorbents, taking into account membrane diffusion, internal diffusion, and surface chemical interactions. Intraparticle diffusion model simplifies the adsorption process into two steps: surface adsorption of the adsorbent and slow diffusion through the pores.

### Numerical simulation

The adsorption kinetics were simulated using COMSOL software to reveal the adsorption property at a micro level. Firstly, the model of capture iodine vapour on ACFs was built (Fig. 2), consisting with the experiment apparatus, and used unstructured mesh (number was 684,474). The ACFs were set as a porous medium. The numerical simulation process of static iodine vapour adsorption on modified ACFs,

which was mainly a porous medium dilute matter transfer process, was mainly driven by the concentration difference between the adsorption vessel and the ACFs. Equation (1) was control equation of dilute matter transfer in porous media, according to the built-in equations of COMSOL software and the law of mass conservation.

$$\frac{\partial(\varepsilon_p c_i)}{\partial t} + \left( \rho \frac{\partial(Kc_i)}{\partial c_i} \frac{\partial c_i}{\partial t} - Kc_i \frac{\rho}{(1 - \varepsilon_p)} \frac{\partial \varepsilon_p}{\partial t} \right) + \nabla \cdot \left( -\varepsilon^{\frac{4}{3}} D_{F,i} \nabla c_i \right) + \mathbf{u} \cdot \nabla c_j = 0 \quad (1)$$

where  $\varepsilon_p$  is porosity of porous media.  $c_i$  is gas phase concentration of substance  $i$ .  $K$  is adsorption coefficient, m<sup>3</sup>/kg.  $\rho$  is bulk density of porous media bed.  $D_{F,i}$  is fluid diffusion coefficient, m<sup>2</sup>/s.  $u$  is velocity vector, m/s. The first term on the left-hand side of Eq. (1) is the variation of iodine concentration in the activated carbon fiber bed over time. The second term represents the amount of iodine adsorbed onto activated carbon fibers over time. The third item is the amount of iodine diffused within the activated carbon fiber bed. The fourth item represents the change in iodine concentration caused by convection.

Table 2 shown the initial and boundary conditions of the control equations. The parameters were performed in COMSOL simulation (Table 3), consisting with experiments results of iodine vapour in ACF-K.

### Molecular simulation

The adsorption isotherms were methodically analyzed to reveal the affection of pore size distribution and temperature on the iodine vapour adsorption in ACFs at a molecular level using Grand canonical Monte Carlo (GCMC) simulation to find the suitable parameters. The single layer slit pore model [32, 33] was used to presence ACFs and iodine was treated as spherical particle [34], as presented in Fig. 3 and Table 4. In this work, the GCMC

**Table 1** The equations and parameters of five kinetics models

Kinetics models	Equation	Parameters
Pseudo-first-order model [32]	$\ln(q_e - q_t) = \ln q_e - k_1 t$	$q_t$ - the adsorption amount at time $t$ , mg/g; $q_e$ - the amount of adsorbed iodine gas at the adsorption equilibrium of activated carbon fiber, mg/g; $k_1$ - the pseudo-first-order adsorption rate constant, min <sup>-1</sup>
Pseudo-second-order model [33]	$\frac{t}{q_t} = \frac{1}{k_2 q_e^2} + \frac{t}{q_e}$	$k_2$ - pseudo-second-order adsorption rate constant, mg/(g·min)
Elovich model [34]	$q_t = \frac{1}{\beta} \ln \alpha \beta - \frac{1}{\beta} \ln t$	$\alpha$ - the initial adsorption rate, mg/(g·min); $\beta$ - the desorption constant, g/mg
Bangham model [35]	$q_t = q_e [1 - \exp(-kt^n)]$	$k$ - the adsorption rate constant, min <sup>-n</sup> ; $n$ - a constant
Intraparticle diffusion model [36]	$q_t = k_{id} t^{\frac{1}{2}} + C$	$k_{id}$ - the rate constant of the diffusion model within the particle, mg/g/min <sup>1/2</sup> ; $C$ - a constant representing the thickness of the boundary layer

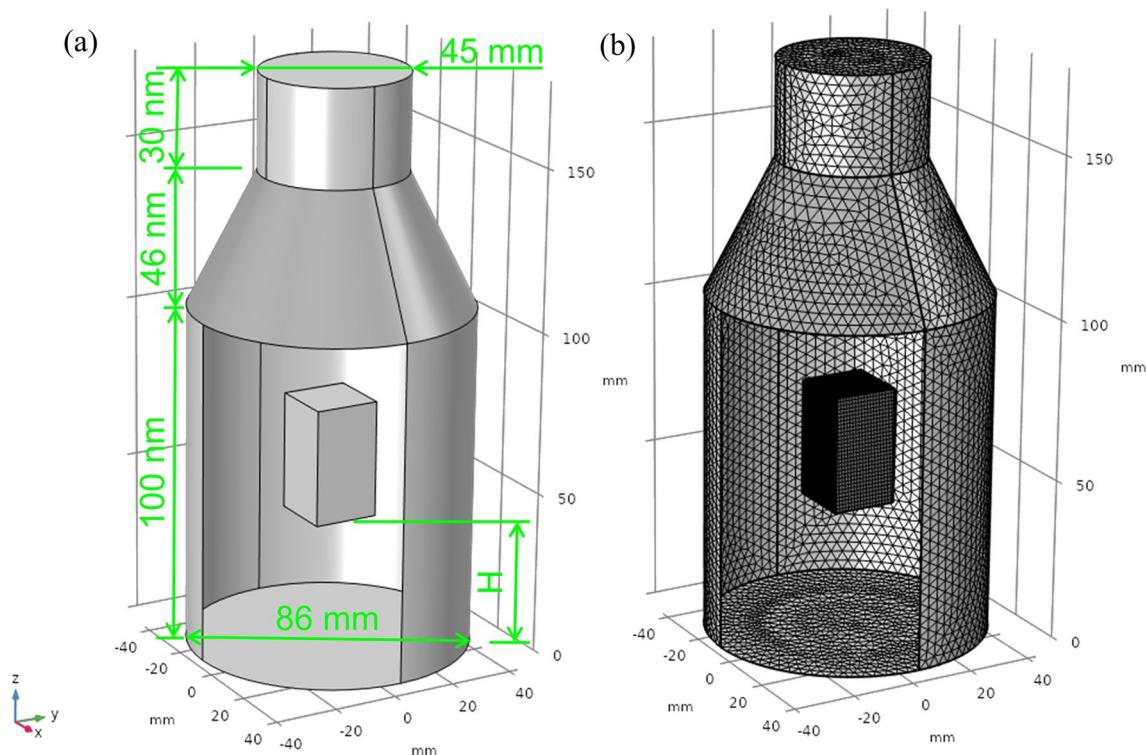


Fig. 2 Schematic diagram of a geometry and b mesh of iodine static adsorption in ACFs

Table 2 Initial and boundary conditions

Boundary type	Setting condition	Remark
Wall surface	$-\vec{n} \cdot \vec{J}_i = 0$	$\vec{n}$ is the direction vector; $J_i$ is the diffusive term
Initial concentration of iodine vapour in ACF	$c_i = 0$	–
Initial concentration of iodine vapour in glass bottle	$c_i = c_0$	$c_0$ is ratio of iodine mass to container volume

Table 3 Parameters set in COMSOL simulation

Parameter	Value	Unit
Adsorption container volume	0.5	L
Loading amount of ACF	1.1	g
Bulk density of ACF	76.389	kg/m <sup>3</sup>
Poriness of ACF	0.64	–
Initial iodine concentration of adsorption vessel	6.4	g/L
Adsorption coefficient of ACF	0.726	m <sup>3</sup> /kg
Diffusion coefficient	$2 \times 10^{-8}$	m <sup>2</sup> /s
Temperature	40	°C

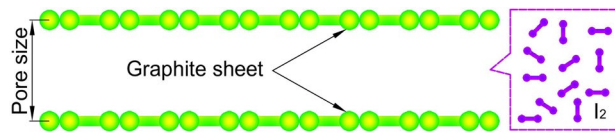


Fig. 3 Schematic diagram of slit pore and iodine models

Table 4 L-J parameters of atoms in ACFs and iodine models

Atom	$\sigma$ (nm)	$\epsilon/k_B$ (K)	References
C	0.3400	28.00	[33]
I <sub>2</sub>	0.4982	550.00	[34]

simulation method was used to capture iodine vapour on ACFs at 40 °C and 1 bar to compare with the experiment results for verifying the model. For each adsorption isotherm, the system equilibration stage was used by  $2 \times 10^7$  Monte Carlo steps, while the adsorption sampling stage was calculated via  $2 \times 10^7$  Monte Carlo steps amid GCMC simulation.

## Results and discussion

### Characterization of ACFs

#### SEM images

The activated carbon fibers before and after modification were scanned by SEM to observe the micro-surface changes, as shown in Fig. 4. The surface of ACF-0 was relatively smooth, while there were many white dot bulges on the surface of modified ACFs, as shown in Fig. 4a–d. Wherein, the surface of ACF-K was relatively rough which had a lot of bulges, and had abundant vermicular stripes, which might be due to the etching of ACF surface caused by the reaction of carbon and potassium hydroxide. The equivalent diameter of ACF-W was 23.5% smaller than that of ACF-0. The surface of ACF-KW also appeared some wormlike stripes and rougher, but the change was not as big as ACF-K. Through the fiber cross section (Fig. 4e–h), it could also be clearly found the degree of erosion after different modification methods was different.

#### N<sub>2</sub> adsorption/desorption isotherms

It can be seen from Fig. 5a that the adsorption isotherms of the samples shown obvious adsorption phenomena at the low pressure region ( $P/P_0 < 0.1$ ), which belonged to the I type isotherms of IUPAC classification. At high pressure, the adsorption desorption hysteresis loop phenomenon occurred,

which was due to the capillary condensation phenomenon of mesoporous adsorption at high pressure. In addition, it can be found that the amount of N<sub>2</sub> adsorption increased after modification, and the amount of nitrogen adsorption on ACF-K was the largest due to form more micropores after the chemical reaction between KOH and C.

As shown in Table 5, the specific surface area ( $S_{\text{BET}}$ ) of the modified ACF had been improved to a certain extent (2.6–8.8%) and the ACF-K had the maximum amount of improvement, which was increased 110 m<sup>2</sup>/g. The specific surface area of micropores ( $S_{\text{micro}}$ ) and micropore volume ( $V_{\text{micro}}$ ) of ACF-K also increased most, which were 69 m<sup>2</sup>/g and 0.04 cm<sup>3</sup>/g, respectively, while the  $S_{\text{micro}}$  and  $V_{\text{micro}}$  of ACF-KW decreased compared with ACF-0 because the combined effect of KOH and microwave led to partial micropore collapse. Comparing with ACF-0, the average pore size ( $D_{\text{average}}$ ) of ACF-K and ACF-KW increased 0.6% and 1.2%, respectively, while ACF-W decreased 2.3%, indicating that KOH and microwave may have the opposite effect on  $D_{\text{average}}$  [17].

#### Elemental analysis

The elements content of ACF-0, ACF-K, ACF-W and ACF-KW were shown in Table 6. C element content of ACF-K and ACF-W increased 2.99% and 1.35%, respectively, and it decreased 9.41% on ACF-KW, confirming that the synergistic KOH and microwave caused largely C to be consumed. After modified activated carbon fiber, N element content increased 10.61–30.30%. S element content of ACF-K and

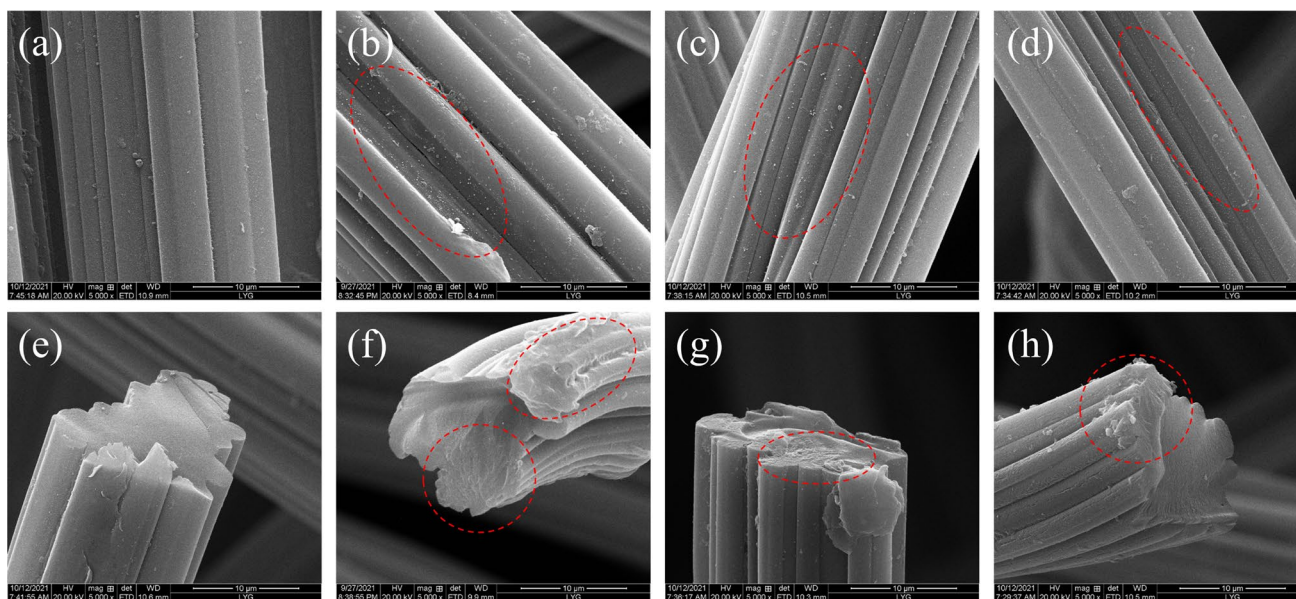


**Fig. 4** SEM images of **a/e** ACF-0, **b/f** ACF-K, **c/g** ACF-W, and **d/h** ACF-KW surface/cross section (Magnification 5000 times, Scale Bar 10 µm)

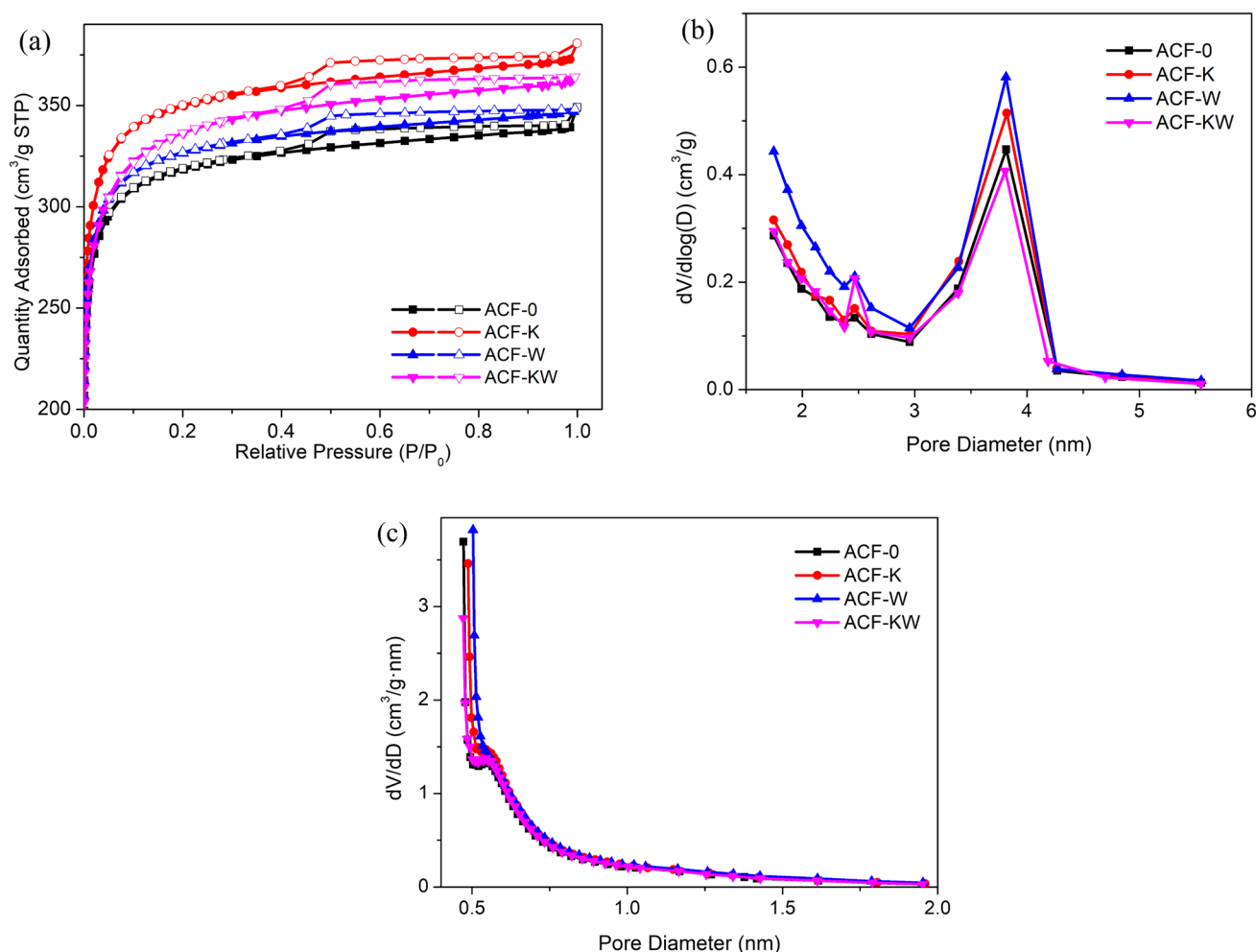


**Fig. 5** **a**  $N_2$  adsorption–desorption isotherms, **b** BJH pore size distribution, and **c** HK pore size distribution of ACF-0, ACF-K, ACF-W and ACF-KW

**Table 5** The textural properties of ACF-0, ACF-K, ACF-W and ACF-KW

Samples	$S_{BET}$ ( $m^2/g$ )	$S_{micro}$ ( $m^2/g$ )	$V_{total}$ ( $cm^3/g$ )	$V_{micro}$ ( $cm^3/g$ )	$D_{average}$ (nm)
ACF-0	1253	896	0.54	0.34	1.72
ACF-K	1363	965	0.59	0.38	1.73
ACF-W	1286	928	0.54	0.36	1.68
ACF-KW	1293	799	0.56	0.32	1.74

**Table 6** Elements content of ACF-0, ACF-K, ACF-W and ACF-KW

Samples	C (%)	N (%)	S (%)	H (%)	Atomic number ratio
ACF-0	63.120	0.660	0.055	3.055	$C_{3.000}N_{0.027}S_{0.001}H_{1.742}$
ACF-K	65.010	0.730	0.793	3.040	$C_{3.000}N_{0.029}S_{0.014}H_{1.683}$
ACF-W	63.970	0.770	0.258	2.347	$C_{3.000}N_{0.031}S_{0.005}H_{1.321}$
ACF-KW	57.180	0.860	0.047	3.190	$C_{3.000}N_{0.039}S_{0.001}H_{2.008}$

ACF-W increased, but it decreased on ACF-KW, while H element content was opposite. Atomic number ratio of the samples did not significantly change after the physical modification at low temperature (40 °C) and short time microwave heating (1 min) in this experiment.

### FT-IR analysis

As shown in Fig. 6, the FTIR spectra of ACF-0, ACF-K, ACF-W and ACF-KW were obtained and compared in the wavenumber range of 4000–500  $cm^{-1}$  to confirm the functional groups and to determine the bond structure. There was a vibration peak due to the existence of crystal water stretching, OH stretching, NH stretching and  $NH_2$  Antisymmetric stretching at 3441  $cm^{-1}$ . CH and  $CH_2$  asymmetric stretching vibration appeared at 2925  $cm^{-1}$ . The vibration peaks at 1622  $cm^{-1}$  and 1081  $cm^{-1}$  were C=C and C–O stretching vibration, respectively. It indicated that ACF

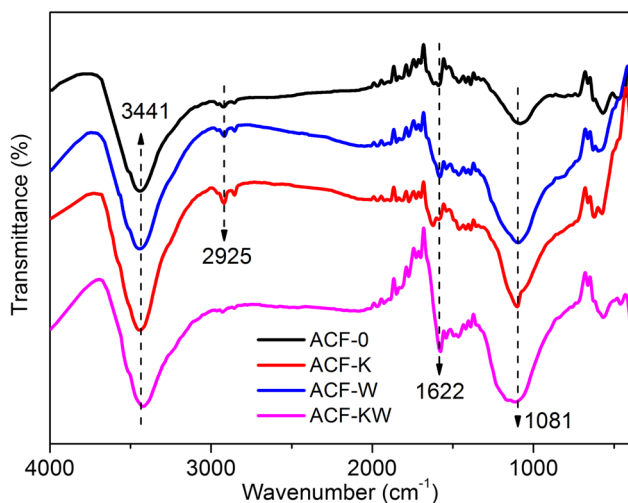


**Fig. 6** FT-IR spectra of ACF-0, ACF-K, ACF-W and ACF-KW

had corresponding functional groups including phenol, amide, ether, alcohol, anhydride and hydroxyl. Noteworthy, the types of functional groups of the ACF-0, ACF-K and ACF-W have no significant change, which could be the result of without high temperature activated ACF-K and the low microwave time of 1 min. Yet the asymmetric stretching vibration at  $2925\text{ cm}^{-1}$  of ACF-KW was disappeared because the dual role of KOH and microwave.

### Adsorption and desorption performance of iodine vapour by modified ACFs

At the initial iodine concentration  $14\text{ g/L}$ , the adsorbents  $1\text{ g}$ , the reactor volume  $500\text{ mL}$ , temperature  $40\text{ }^{\circ}\text{C}$  and  $1\text{ bar}$ , the iodine adsorption kinetics curve and iodine adsorption amount of four materials were obtained (Fig. 7).

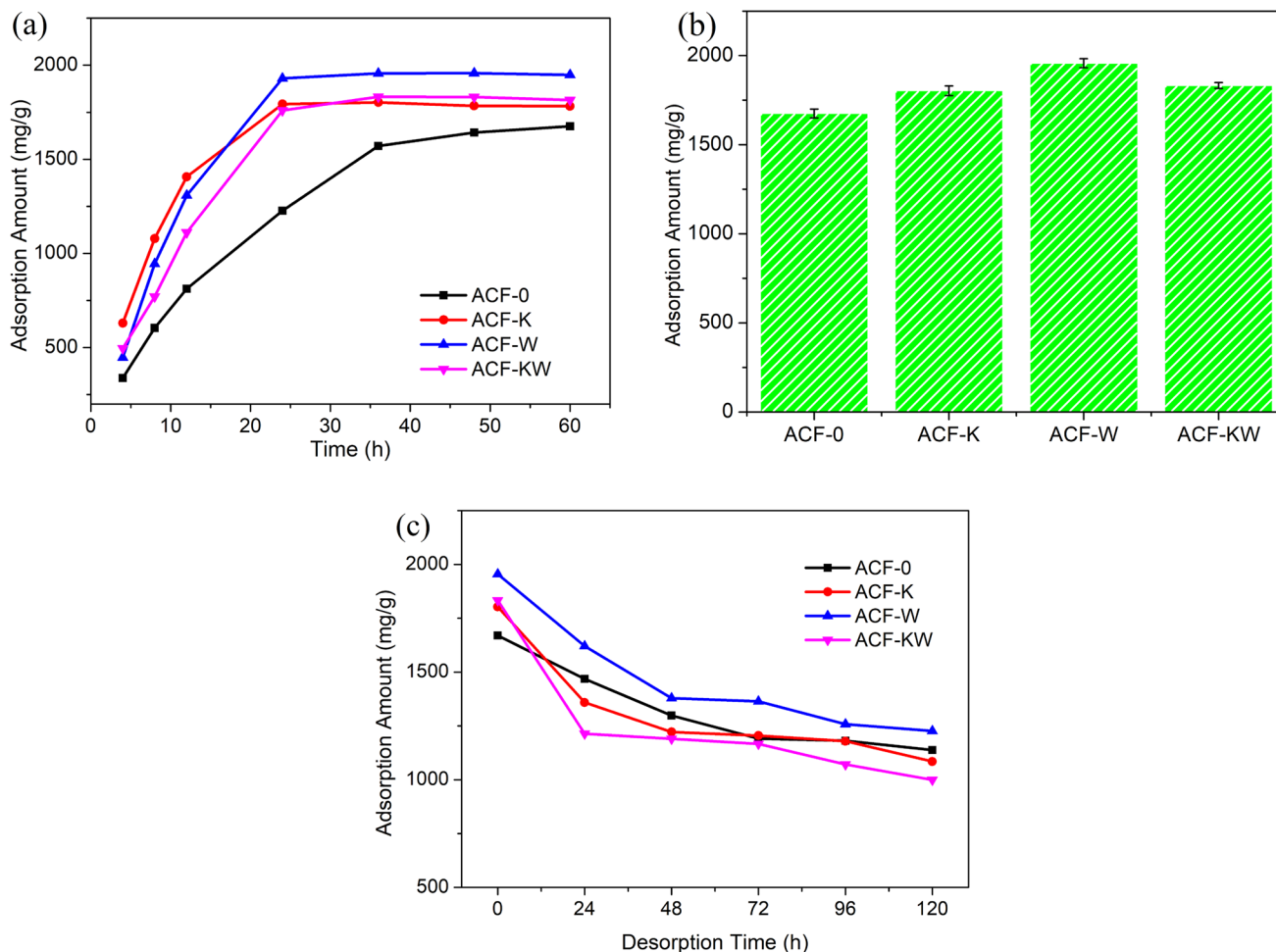


**Fig. 7** **a** Iodine adsorption kinetics curve at  $40\text{ }^{\circ}\text{C}$  and  $1\text{ bar}$  and **b** iodine adsorption amount of ACF-0, ACF-K, ACF-W and ACF-KW. ( $C_{\text{iodine}} = 14\text{ g/L}$ ,  $m_{\text{adsorbent}} = 1\text{ g}$ , and  $V_{\text{reactor}} = 500\text{ mL}$ , Error

bars = standard deviation of three parallel experiments). **c** Iodine desorption experiment results

### Adsorption and desorption of iodine vapour on ACF-K

Figure 7 shown that the modified activated carbon fiber adsorption of iodine vapour has obviously changed. At 12 h and 24 h, the instantaneous iodine adsorption amount of ACF-K was 1407 mg/g and 1794 mg/g, respectively. The instantaneous iodine adsorption amount of unmodified ACF was 812 mg/g and 1227 mg/g, respectively. Compared with the unmodified activated carbon fiber, the gas iodine adsorbed by the modified activated carbon fiber increased by 596 mg/g and 566 mg/g at 12 h and 24 h, respectively, with an increase of 73% and 46%, respectively. At the same time, the adsorption rate of modified ACF was greatly accelerated, and the time required to reach the adsorption equilibrium was reduced by 50% compared with that without modification (Fig. 7a). After 24, 48, 72, 96 and 120 h of desorption (Fig. 7c), the adsorption amount and the iodine retention rate of ACF-K was 1359, 1222, 1205, 1179 and 1085 mg/g, and the iodine retention rate of it was 75.4%, 67.8%, 66.8%, 65.4% and 60.2%, respectively.

### Adsorption and desorption of iodine vapour on ACF-W

Adsorption rate of iodine vapour on activated carbon fiber modified by microwave increased by 50% (Fig. 7a). Compared with ACF-0, ACF-K and ACF-KW, the iodine equilibrium adsorption amount of ACF-W was the highest up to 1958 mg/g, which increased 16.8% on that of unmodified activated carbon fiber (1675 mg/g) as shown in Fig. 7b. The adsorption amount of ACF-W was also the highest of the adsorbents after 24, 48, 72, 96 and 120 h of desorption

**Table 7** Summary of iodine vapour adsorption amount results on different adsorbents

Adsorbents	Iodine state	Temperature (°C)	$q$ (mg/g)	References
SR-KOH	Gaseous	80	6460	[37]
Catechin@ACF	Gaseous	75	2123	[15]
ACF-W	Gaseous	40	1958	This work
ACF-KW	Gaseous	40	1832	This work
ACF-K	Gaseous	40	1803	This work
ACF-0	Gaseous	40	1675	This work
ZIF-8@wood	Gaseous	75	1090	[38]
Bi <sub>2</sub> O <sub>3</sub> @g-C <sub>3</sub> N <sub>4</sub>	Gaseous	100	830	[29]
CF/COF	Gaseous	77	824	[39]
MOF membrane	Gaseous	125	610	[2]
COFs@cotton	Gaseous	77	534	[40]

(Fig. 7c), which was 1621, 1379, 1364, 1258 and 1227 mg/g, and the iodine retention rate of it was 82.9%, 70.5%, 69.8%, 64.3% and 62.8%, respectively. Under the experiment condition, microwave modified ACFs was an effective material for the iodine capture, because the microwave modified method increased the iodine adsorption amount and iodine retention performance.

### Adsorption and desorption of iodine vapour on ACF-KW

The iodine equilibrium adsorption amount of ACF-KW was between ACF-K and ACF-W presented in Fig. 7b. This shown that the combination of the two technologies does not increase the amount of adsorption due to the pore structure

**Table 8** The results of kinetics models fit with experiment data of ACF-0, ACF-K, ACF-W and ACF-KW to iodine vapour

Types of kinetics	Parameter	ACF-0	ACF-K	ACF-W	ACF-KW
Pseudo-first-order model	$q_e$ experimental value	1675	1803	1958	1832
	$q_e$	1790	1824	2035	1910
	$k_1$	0.0512	0.1166	0.0839	0.0762
	$R^2$	0.9961	0.9907	0.9802	0.9787
Pseudo-second-order model	$q_e$	2410	2120	2513	2392
	$k_2$	1.8115	6.5234	3.3418	3.113
	$R^2$	0.9914	0.9496	0.9459	0.9521
Elovich model	$\alpha$	226.79	668.33	393.56	347.52
	$\beta$	0.0019	0.0023	0.0017	0.0018
	$R^2$	0.9853	0.8898	0.9208	0.9321
Bangham channel model	$q_e$	1770	1802	1968	1852
	$k$	0.0485	0.0781	0.0344	0.0421
	$n$	1.0275	1.1990	1.4120	1.2697
	$R^2$	0.9963	0.9971	0.9977	0.9892
Intraparticle diffusion model	$k_{id}$	245.74	185.69	255.03	243.50
	$C$	-64.57	570.22	265.35	195.74
	$R^2$	0.9605	0.7618	0.8118	0.8498



(Table 5) and surface chemical (Table 6 and Fig. 6). But after 24, 48, 72, 96 and 120 h of desorption (Fig. 7c), the adsorption amount of ACF-KW was the lowest of the adsorbents, which was 1214, 1190, 1167, 1071 and 1000 mg/g, and the iodine retention rate of it was 66.2%, 64.9%, 63.6%, 58.4%, and 54.5%, respectively.

Since the modified ACFs can capture iodine vapour effectively, their adsorption amount was compared with other reported adsorbents. As can be seen in Table 7, although the equilibrium adsorption amount of modified ACFs were less than those of SR-KOH and Catechin@ACF, the preparation method and cost of ACFs were simpler and lower than those of SR-KOH and Catechin@ACF. The advantage of modified ACFs was used at normal ventilation temperature (40 °C), while  $\text{Bi}_2\text{O}_3$ @g- $\text{C}_3\text{N}_4$  and MOF membrane was used at high temperature (100 °C and 125 °C).

## Adsorption kinetics

To evaluate adsorption property of iodine vapour on ACFs, the experimental data were plotted and fitted using kinetics models (Table 1). In order to determine the best model to describe the experimental data, the following evaluation factors were considered: the adsorption amount  $q_e$  and the determination coefficient ( $R^2$ ) and the fitting results were shown in Table 8 and Fig. 8.

From the correlation coefficient  $R^2$ , the order of the adsorption process and model fit was Bangham (0.9963) > pseudo-first-order (0.9961) > pseudo-second-order (0.9914) > Elovich (0.9853) > Intraparticle diffusion model (0.9605). It indicated that the adsorptive behavior was better represented by the Bangham channel model and pseudo-first-order model. As can be seen from  $q_e$ , the error between the fitted  $q_e$  value of the Bangham model and the experimental value was the minimum. It implied that

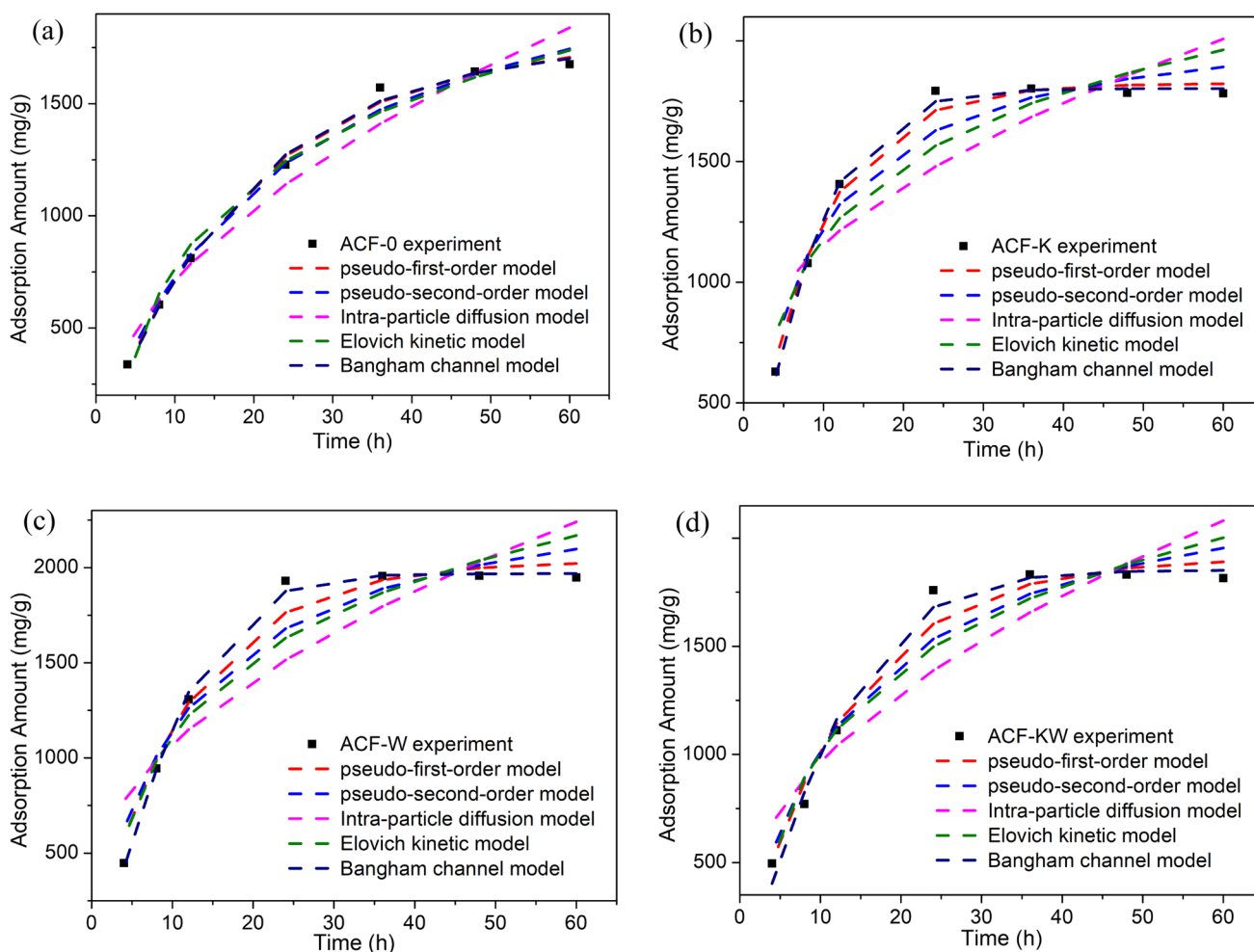


**Fig. 8** Kinetics models fit for iodine vapour absorption experiment data on **a** ACF-0, **b** ACF-K, **c** ACF-W, and **d** ACF-KW

the adsorption of iodine gas by activated carbon fiber was mainly surface physical adsorption of micropores. This is also in line with the cognitive theory that activated carbon fiber adsorption of iodine gas is mainly physical adsorption.

### Numerical simulation results

The COMSOL was used to reveal the relationship between ACFs parameters (density, adsorption coefficient and poriness) and adsorption function at a micro level. From Fig. 9a it can be seen that numerical simulation and experimental data of iodine vapour adsorption on ACF-K matched well, with relative errors range of 2.0–9.2% which met actual project requirements of less than 10%.

The effect of ACFs density (56.389 kg/m<sup>3</sup>, 66.389 kg/m<sup>3</sup>, 76.389 kg/m<sup>3</sup>, 86.389 kg/m<sup>3</sup> and 96.389 kg/m<sup>3</sup>) on iodine vapour adsorption amount was analyzed using numerical simulation. Figure 9b shows that the iodine adsorption amount decreased with increasing of ACFs density,

which may be due to that effective adsorption process was adversely affected by closely overlapped of ACFs.

The effect of ACFs adsorption coefficient (0.526 m<sup>3</sup>/kg, 0.626 m<sup>3</sup>/kg, 0.726 m<sup>3</sup>/kg, 0.826 m<sup>3</sup>/kg, and 0.926 m<sup>3</sup>/kg) on iodine vapour adsorption amount was measured by numerical simulation. As shown in Fig. 9c, the iodine adsorption amount dramatically increased with increasing of ACFs adsorption coefficient, indicating adsorption coefficient was an important parameter to measure the adsorption performance on ACF.

The effect of ACFs poriness (0.44, 0.54, 0.64, 0.74, and 0.84) on iodine vapour adsorption amount was performed via numerical simulation. Iodine equilibrium adsorption amount were almost equal under different porosity, while the adsorption rates slight increased with increasing of ACFs poriness displayed in Fig. 9d.

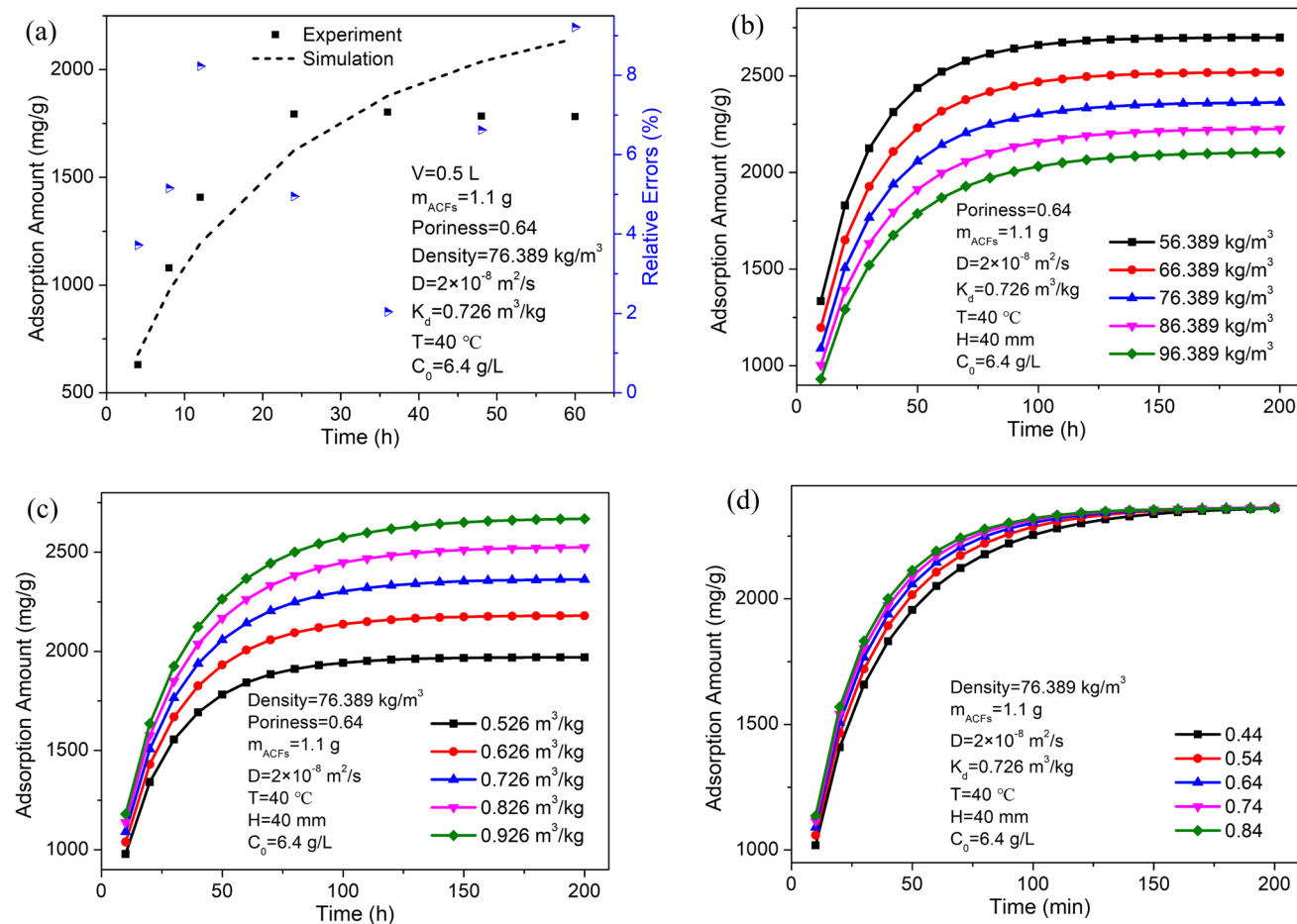


**Fig. 9** a Validation of numerical simulation at the adsorption process by COMSOL software. The effect of **b** density, **c** adsorption coefficient, and **d** poriness on the iodine vapour adsorption in ACFs

## Molecular simulation results

GCMC simulation was performed to study the adsorption isotherm of the iodine in a series of ACFs slit-like pore models at molecular level, which were built using the BJH pore size distribution data (Fig. 5b) of the real adsorbent (ACF-0, ACF-K, ACF-W and ACF-KW), including 1.7 nm, 1.9 nm, 2.0 nm, 2.1 nm, 2.2 nm, 2.4 nm, 2.5 nm, 2.6 nm, 3.0 nm, 3.4 nm and 3.8 nm. Iodine adsorption simulation results (Fig. 10a) of ACF-0, ACF-K, ACF-W and ACF-KW were calculated using weighted average of adsorption amount in different pore sizes up to 1933 mg/g, 1931 mg/g, 1930 mg/g and 1933 mg/g, respectively, comparing with that of experimental data 1675 mg/g, 1803 mg/g, 1958 mg/g and 1832 mg/g (relative error in the range of 0.7–2%), which was validated the reliability of the models and GCMC method (Fig. 10b).

Then the effect of pore sizes, which were chosen according to the BJH and HK results (Fig. 5c) of ACF-K from

$N_2$  adsorption–desorption isotherm, on the iodine vapour adsorption were analyzed. Figure 10c shown that the top four iodine vapour adsorption amount were obtained at 1.6 nm, 1.7 nm, 1.8 nm and 1.9 nm, which were the optimal pore sizes for iodine adsorption at 40 °C and 1 bar. The iodine uptakes were increased step by step with the pore sizes increasing from 0.7 nm to 1.4 nm. The iodine adsorption amount of 2.0 nm was rapidly increased with increasing pressure, while the iodine adsorption isotherms of 2.5 nm, 3.0 nm and 3.8 nm were basically overlapped with that of 1.3 nm. It was found that both too large and too small pore sizes were not conducive to iodine vapour adsorption, existing optimal adsorption pore sizes, which can effectively guide preparation of adsorbents.

The iodine adsorption isotherms were studied under five temperatures (20 °C, 40 °C, 60 °C, 80 °C, and 100 °C) as shown in Fig. 10d. Obviously, the iodine vapour adsorption amount were decreased with increasing of temperature.

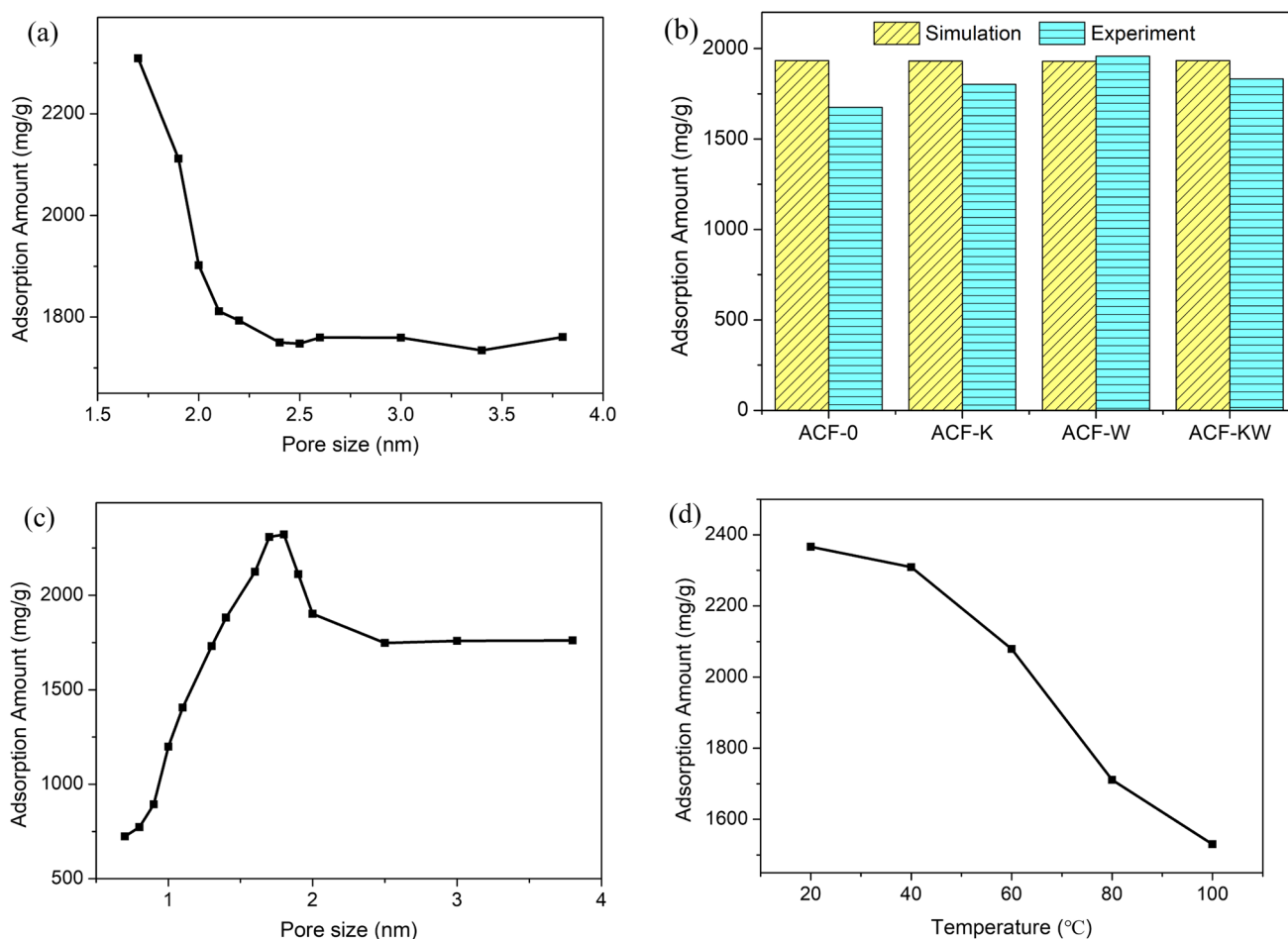


**Fig. 10** a Iodine adsorption simulation results at 1 bar and b comparison of weighted average of the simulated adsorption amount and experimental data to validation of models of ACFs and iodine at the

adsorption process by GCMC method. The effect of c pore size and d temperature on the iodine vapour adsorption amount in ACFs

## Conclusion

Both experiment and simulation methods were used to reveal the iodine vapour adsorption mechanism on modified ACFs at micro and molecular levels. In this study, viscose-based activated carbon fiber was modified by three technologies and the performance of adsorption iodine vapour on the ACFs was analyzed. After modification, the maximum specific surface area of ACFs was 1363 m<sup>2</sup>/g (ACF-K) and the maximum saturated adsorption iodine gas amounts was 1958 mg/g (ACF-W), indicating that the adsorption amount was not proportional to the specific surface area. The conclusion had also been verified at the molecular level by the GCMC simulation results that the optimum iodine vapour adsorption pore size range of ACFs was between 1.6 and 1.9 nm at 40 °C and 1 bar. It is critically important to design adsorbent for removing iodine with a vast amount of effective pore size. Meanwhile, the adsorption rate of iodine gas on activated carbon fibers after the above modification methods increased by 50% due to the changes of pore structure and chemical characteristics, which is consistent with the COMSOL simulation results that the most promising ACFs parameters were lower density, higher adsorption coefficient and taller porosity. Bangham and pseudo-first-order kinetics models were the best fit with all of the iodine adsorption kinetics curve of experiment, indicating that the main adsorption was physisorption which also verified at the molecular level.

In the future, the experiments and simulations of breakthrough adsorption at different condition and affection of functional groups will be studied to systematically predict the behavior of iodine adsorption in ACFs. Meanwhile, the influence of the sequence of the preparation steps on the results is being done and will continue in future work.

**Acknowledgements** This work was supported by the National Natural Science Foundation of China (Grant Number 12275122 and U1867221).

## Declarations

**Conflict of interest** The authors declare that they have no known competing financial interests or personal relationships that could have appeared to influence the work reported in this paper.

## References

- Nandanwar SU, Coldsnow K, Utgikar V, Sabharwall P, Aston DE (2016) Capture of harmful radioactive contaminants from off-gas stream using porous solid sorbents for clean environment - a review. *Chem Eng J* 306:369–381. <https://doi.org/10.1016/j.cej.2016.07.073>
- Li M, Yuan G, Zeng Y, Yang Y, Liao J, Yang J, Liu N (2020) Flexible surface-supported MOF membrane via a convenient approach for efficient iodine adsorption. *J Radioanal Nucl Chem* 324:1167–1177. <https://doi.org/10.1007/s10967-020-07135-3>
- Nandanwar SU, Coldsnow K, Porter A, Sabharwall P, Aston DE, McIlroy DN, Utgikar V (2017) Adsorption of radioactive iodine and krypton from off-gas stream using continuous flow adsorption column. *Chem Eng J* 320:222–231. <https://doi.org/10.1016/j.cej.2017.03.020>
- Yang X, Xie D, Wang W, Li S, Tang Z, Dai S (2023) An activated carbon from walnut shell for dynamic capture of high concentration gaseous iodine. *Chem Eng J* 454:140365. <https://doi.org/10.1016/j.cej.2022.140365>
- Umadevi K, Mandal D (2021) Performance of radio-iodine discharge control methods of nuclear reprocessing plants. *J Environ Radioact* 234:106623. <https://doi.org/10.1016/j.jenvrad.2021.106623>
- Sakurai T, Takahashi A, Ye M, Kihara T, Fujine S (1997) Trapping and measuring radioactive (iodine-129) in cartridge filters. *J Nucl Sci Technol* 34:211–216. <https://doi.org/10.1080/18811248.1997.9733648>
- Mineo H, Gotoh M, Iizuka M, Fujisaki S, Uchiyama G (2002) A simple model predicting iodine profile in a packed bed of silica-gel impregnated with silver nitrate. *J Nucl Sci Technol* 39:241–247. <https://doi.org/10.1080/18811248.2002.9715181>
- Mineo H, Gotoh M, Iizuka M, Fujisaki S, Hagiya H, Uchiyama G (2003) Applicability of a model predicting iodine-129 profile in a silver nitrate silica-gel column for dissolver off-gas treatment of fuel reprocessing. *Sep Sci Technol* 38:1981–2001. <https://doi.org/10.1081/SS-120020130>
- Wu L, Sawada JA, Kuznicki DB, Kuznicki T, Kuznicki SM (2014) Iodine adsorption on silver-exchanged titania-derived adsorbents. *J Radioanal Nucl Chem* 302:527–532. <https://doi.org/10.1007/s10967-014-3252-5>
- Sava DF, Chapman KW, Rodriguez MA, Greathouse JA, Crozier PS, Zhao H, Chupas PJ, Nenoff TM (2013) Competitive I<sub>2</sub> sorption by Cu-BTC from humid gas streams. *Chem Mater* 25:2591–2596. <https://doi.org/10.1021/cm401762g>
- Subrahmanyam KS, Sarma D, Malliakas CD, Polychronopoulou K, Riley BJ, Pierce DA, Chun J, Kanatzidis MG (2015) Chalcogenide aerogels as sorbents for radioactive iodine. *Chem Mater* 27:2619–2626. <https://doi.org/10.1021/acs.chemmater.5b00413>
- Su K, Wang W, Li B, Yuan D (2018) Azo-bridged calix[4]resorcinarene-based porous organic frameworks with highly efficient enrichment of volatile iodine. *ACS Sustain Chem Eng* 6:17402–17409. <https://doi.org/10.1021/acssuschemeng.8b05203>
- Katsoulidis AP, He J, Kanatzidis MG (2012) Functional monolithic polymer organic framework aerogel as reducing and hosting media for Ag nanoparticles and application in capturing of iodine vapors. *Chem Mater* 24:1937–1943. <https://doi.org/10.1021/cm300696g>
- Jiao F, Sang H, Guo P, Miao P, Wang X (2022) Efficient adsorption and porous features from activated carbon felts activated by the eutectic of Na<sub>2</sub>CO<sub>3</sub> and K<sub>2</sub>CO<sub>3</sub> with vapor. *Chem Phys Lett* 803:139831. <https://doi.org/10.1016/j.cplett.2022.139831>
- Zhu H, Wang B, Zhu W, Duan T, He G, Wei Y, Sun D, Zhou J (2022) Interface assembly of specific recognition gripper wrapping on activated collagen fiber for synergistic capture effect of iodine. *Colloids Surf B* 210:112216. <https://doi.org/10.1016/j.colsurfb.2021.112216>
- Yu M, Li Z, Ji Q, Wang S, Su D, Lin Y (2009) Effect of thermal oxidation of activated carbon surface on its adsorption towards dibenzothiophene. *Chem Eng J* 148:242–247. <https://doi.org/10.1016/j.cej.2008.08.018>
- Valente Nabais JM, Carrott PJM, Ribeiro Carrott MML, Menendez JA (2004) Preparation and modification of activated carbon

- fibres by microwave heating. *Carbon* 42:1315–1320. <https://doi.org/10.1016/j.carbon.2004.01.033>
18. Liu Q, Zheng T, Li N, Wang P, Abulikemu G (2010) Modification of bamboo-based activated carbon using microwave radiation and its effects on the adsorption of methylene blue. *Appl Surf Sci* 256:3309–3315. <https://doi.org/10.1016/j.apsusc.2009.12.025>
  19. Bhatnagar A, Hogland W, Marques M (2013) An overview of the modification methods of activated carbon for its water treatment applications. *Chem Eng J* 219:499–511. <https://doi.org/10.1016/j.cej.2012.12.038>
  20. Gong S, Sun Y, Zheng K, Jiang G, Li L, Feng J (2020) Degradation of levofloxacin in aqueous solution by non-thermal plasma combined with  $\text{Ag}_3\text{PO}_4$ /activated carbon fibers: mechanism and degradation pathways. *Sep Purif Technol* 250:117264. <https://doi.org/10.1016/j.seppur.2020.117264>
  21. Mangun CL, Benak KR, Economy J, Foster KL (2001) Surface chemistry, pore sizes and adsorption properties of activated carbon fibers and precursors treated with ammonia. *Carbon* 39:1809–1820. [https://doi.org/10.1016/S0008-6223\(00\)00319-5](https://doi.org/10.1016/S0008-6223(00)00319-5)
  22. Chiang H, Huang C, Chiang P (2002) The surface characteristics of activated carbon as affected by ozone and alkaline treatment. *Chemosphere* 47:257–265. [https://doi.org/10.1016/S0045-6535\(01\)00215-6](https://doi.org/10.1016/S0045-6535(01)00215-6)
  23. Aguilera PG, Gutiérrez Ortiz FJ (2016) Prediction of fixed-bed breakthrough curves for  $\text{H}_2\text{S}$  adsorption from biogas: Importance of axial dispersion for design. *Chem Eng J* 289:93–98. <https://doi.org/10.1016/j.cej.2015.12.075>
  24. Shafeeyan MS, Daud WMAW, Shamiri A, Aghamohammadi N (2015) Modeling of carbon dioxide adsorption onto ammonia-modified activated carbon: kinetic analysis and breakthrough behavior. *Energy Fuels* 29:6565–6577. <https://doi.org/10.1021/acs.energyfuels.5b00653>
  25. Zhao H, Bahamon D, Khaleel M, Vega LF (2022) Insights into the performance of hybrid graphene oxide/MOFs for  $\text{CO}_2$  capture at process conditions by molecular simulations. *Chem Eng J* 449:137884. <https://doi.org/10.1016/j.cej.2022.137884>
  26. Liu B, Yu L, Wang H, Ma X, Zeng Z, Li L (2022) Experimental and molecular perspective on VOCs adsorption and separation: Study of the surface heterogeneity and oxygen functionalizing. *Chem Eng J* 435:135069. <https://doi.org/10.1016/j.cej.2022.135069>
  27. Jia M, Rong S, Su P, Li W (2022) Designing functional terminals and vacancies into crystalline porous materials for iodine capture. *Chem Eng J* 437:135432. <https://doi.org/10.1016/j.cej.2022.135432>
  28. Lin Z, Liu L, Liu C, Gao X (2021) Adsorptive separation of Xe/Kr using nanoporous carbons in the presence of  $\text{I}_2$  and  $\text{CH}_3\text{I}$ . *Sep Purif Technol* 275:119161. <https://doi.org/10.1016/j.seppur.2021.119161>
  29. Reda AT, Zhang D, Xu X, Xu S (2022) Highly stable iodine capture by pillared montmorillonite functionalized  $\text{Bi}_2\text{O}_3$ @g- $\text{C}_3\text{N}_4$  nanosheets. *Sep Purif Technol* 292:120994. <https://doi.org/10.1016/j.seppur.2022.120994>
  30. Wang J, Li M, Feng Y, Liu Y, Liu J (2022) Efficient capture of radioactive iodine by Ag-attached silica gel and its kinetics. *Nucl Mater Energy* 33:101270. <https://doi.org/10.1016/j.nme.2022.101270>
  31. Zhou J, Lan T, Li T, Chen Q, Bai P, Liu F, Yuan Z, Zheng W, Luo X, Yan W, Yan T (2022) Highly efficient capture of iodine in spent fuel reprocessing off-gas by novel porous copper-doped silica zeolites. *Sep Purif Technol* 290:120895. <https://doi.org/10.1016/j.seppur.2022.120895>
  32. Zhao Y, Li J, Chen L, Guo Q, Li L, Chai Z, Wang S (2023) Efficient removal of iodide/iodate from aqueous solutions by Purolite A530E resin. *J Radioanal Nucl Chem* 332:1193–1202. <https://doi.org/10.1007/s10967-023-08786-8>
  33. Sari A, Tuzen M, Citak D, Soylak M (2007) Equilibrium, kinetic and thermodynamic studies of adsorption of Pb (II) from aqueous solution onto Turkish kaolinite clay. *J Hazard Mater* 149:283–291. <https://doi.org/10.1016/j.jhazmat.2007.03.078>
  34. Liu Q, Zhou Y, Wang M, Zhang Q, Ji T, Chen T, Yu D (2019) Adsorption of methylene blue from aqueous solution onto viscose-based activated carbon fiber felts: Kinetics and equilibrium studies. *Adsorp Sci Technol* 37:312–332. <https://doi.org/10.1177/0263617419827437>
  35. Kavitha D, Namasivayam C (2007) Experimental and kinetic studies on methylene blue adsorption by coir pith carbon. *Bioresour Technol* 98:14–21. <https://doi.org/10.1016/j.biortech.2005.12.008>
  36. Wu F, Tseng R, Juang R (2009) Initial behavior of intraparticle diffusion model used in the description of adsorption kinetics. *Chem Eng J* 153:1–8. <https://doi.org/10.1016/j.cej.2009.04.042>
  37. Sun H, Yang B, Li A (2019) Biomass derived porous carbon for efficient capture of carbon dioxide, organic contaminants and volatile iodine with exceptionally high uptake. *Chem Eng J* 372:65–73. <https://doi.org/10.1016/j.cej.2019.04.061>
  38. Wang Z, He Y, Zhu L, Zhang L, Liu B, Zhang Y, Duan T (2021) Natural porous wood decorated with ZIF-8 for high efficient iodine capture. *Mater Chem Phys* 258:123964. <https://doi.org/10.1016/j.matchemphys.2020.123964>
  39. Li L, Chen R, Li Y, Xiong T, Li Y (2020) Novel cotton fiber-covalent organic framework hybrid monolith for reversible capture of iodine. *Cellulose* 27:5879–5892. <https://doi.org/10.1007/s10570-020-03189-4>
  40. Li Y, Li Y, Zhao Q, Li L, Chen R, He C (2019) Cotton fiber functionalized with 2D covalent organic frameworks for iodine capture. *Cellulose* 27:1517–1529. <https://doi.org/10.1007/s10570-019-02877-0>
- Publisher's Note** Springer Nature remains neutral with regard to jurisdictional claims in published maps and institutional affiliations.
- Springer Nature or its licensor (e.g. a society or other partner) holds exclusive rights to this article under a publishing agreement with the author(s) or other rightsholder(s); author self-archiving of the accepted manuscript version of this article is solely governed by the terms of such publishing agreement and applicable law.